THE JOURNAL OF PHYSICAL CHEMISTRY A
A JOURNAL OF THE AMERICAN CHEMICAL SOCIETY

pubs.acs.org/JPCA Article

Photodissociation Dynamics of H_2O via the $\tilde{E}'$ ($^1B_2$) Electronic State

Published as part of The Journal of Physical Chemistry virtual special issue "Cheuk-Yiu Ng Festschrift".

Zijie Luo,[‖] Yao Chang,[‖] Yarui Zhao, Jiayue Yang, Zhichao Chen, Yi Cheng, Li Che, Guorong Wu, Xueming Yang,* and Kaijun Yuan*

Cite This: https://doi.org/10.1021/acs.jpca.1c01459 Read Online

ACCESS | Metrics & More | Article Recommendations

ABSTRACT: Photodissociation dynamics of H_2O via the $\tilde{E}'^1B_2$ state were studied using the high-resolution H atom photofragment translational spectroscopy method, in combination with the tunable vacuum ultraviolet free electron laser (VUV FEL). The measured translational energy spectra allow us to determine the respective quantum state population distributions for the nascent OH($X^2\Pi$) and OH($A^2\Sigma^+$) photofragments. Analyses of the quantum state population distributions show both the ground and electronically excited OH fragments to be formed with moderate vibrational excitation but with highly rotational excitation. Unlike the dissociation via the lower-lying electronic states, where OH(X) is the major fragment, the OH(A) products are predominant via the $\tilde{E}'$ state. These products are mainly ascribed to a fast dissociation on the $\tilde{B}^1A_1$ state surface after nonadiabatic transitions from the initial excited $\tilde{E}'$ state to the $\tilde{B}$ state. Meanwhile, another dissociation pathway from the $\tilde{E}'$ state to the $^1B_2$ $3pb_2$ state, followed by coupling to the $^1A_2$ $3pb_2$ state, is also observed, which yields the OH(X) + H and O(^3P) + 2H products.

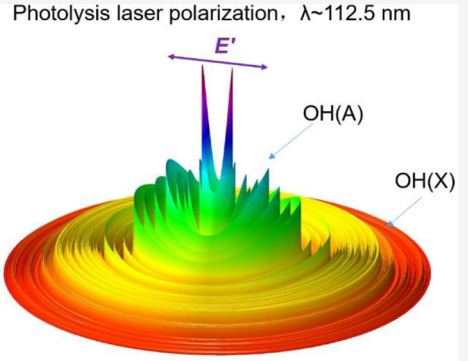

1. INTRODUCTION

Photodissociation of the water molecule in the vacuum ultraviolet (VUV) region has attracted much attention in the last 30 years, since its significance was demonstrated in interstellar chemistry and atmospheric chemistry.[1−3] The molecular orbital configuration of water in its C_{2v} symmetry ground state is $(core)^2(1a_1)^2(2a_1)^2(3a_1)^2(1b_1)^2$, $\tilde{X}^1A_1$. Its VUV absorption spectrum can be divided into four main regions between 190 and 120 nm, as shown in Figure 1.[4] The first broad continuum near 190−140 nm is ascribed as the electronic transition $\tilde{A}^1B_1 \leftarrow \tilde{X}^1A_1$ ($3sa_1 \leftarrow 1b_1$), while the second continuum centered around 128 nm which shows some diffuse vibrational structures corresponds to the electronic transition $\tilde{B}^1A_1 \leftarrow \tilde{X}^1A_1$ ($3sa_1 \leftarrow 3a_1$).[5] In addition, the narrow peaks at around 124 and 122 nm are attributed to the $3p$ Rydberg transitions, $\tilde{C}^1B_1 \leftarrow \tilde{X}^1A_1$ ($3pa_1 \leftarrow 1b_1$) and $\tilde{D}^1A_1 \leftarrow \tilde{X}^1A_1$ ($3pa_2 \leftarrow 1b_1$), respectively.[6]

During the past few decades, extensive experimental and theoretical studies have been performed on this system. Dissociation of H_2O molecules on the $\tilde{A}$ state illustrates a fast direct dissociation, due to the repulsive potential energy surface (PES) along the O−H bond, which yields a H atom plus a ground state OH($X^2\Pi$) with moderate vibrational and cold rotational excitation.[7−15] In contrast, the dissociation dynamics from the $\tilde{B}$ state is fairly intricate because of the complexity of its PES and various nonadiabatic couplings between the $\tilde{B}$ state and the lower-lying states.[16−23] Direct

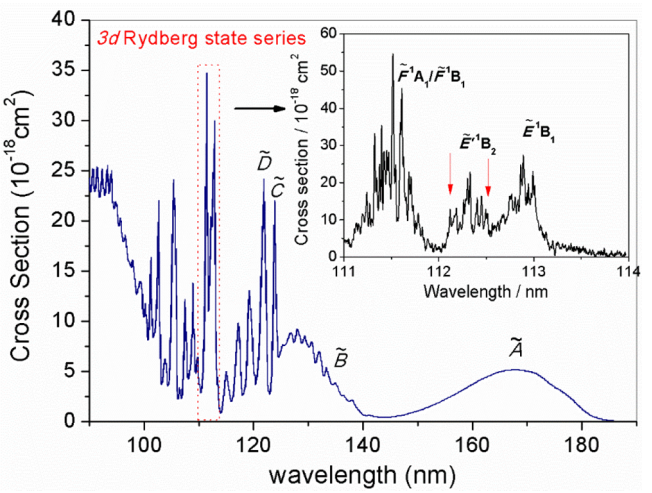

Figure 1. Absorption spectrum of a room temperature sample of H_2O vapor (adapted from ref 4). The spectrum around 114−111 nm with high resolution is adapted from ref 54. The excited electronic states have been marked in the figures. The photolysis wavelengths applied in this work are marked by red arrows.

Received: February 17, 2021
Revised: April 13, 2021

dissociation on this surface leads to electronically excited $OH(A^2\Sigma^+)$ products. However, the major pathway leads to a H atom plus a ground state OH(X) molecule via nonadiabatic crossing from the $\tilde{B}$ state to the PESs of either the $\tilde{A}$ state or the ground state of $H_2O(\tilde{X}^1A_1)$ at the linear geometry. In both cases, the OH products are highly rotationally excited, but with limited vibrational excitation.[24−32] These detailed dissociation dynamics have been exhibited at the Lyman-α wavelength (121.6 nm) photolysis.[33−36] Yang and co-workers reported striking even−odd rotational state population oscillations for the OH(X, v = 0) products.[33,34] These oscillations had been attributed to the dynamical interference between the two conical intersection (CI) pathways between the $\tilde{B}$ and $\tilde{X}$ state surfaces at linear HOH and HHO configurations.[37−39]

The next two excited states have a predominant Rydberg character, named $\tilde{C}$ and $\tilde{D}$ states, which predissociate through nonadiabatic coupling to the lower-lying states. The predissociation rate of the $\tilde{C}$ state is relatively slow, and a resolvable rotational structure at $\lambda \sim 124$ nm can be observed.[40−45] Previous studies have identified that the dissociation dynamics of the $\tilde{C}$ state depends strongly on the excited rotational quantum number.[46−50] Dissociation from $\tilde{C}$ state rotational levels with $\langle J_a \rangle^2 = 0$ occurs exclusively through the homogeneous (vibronic) coupling to the $\tilde{A}$ state, yielding highly vibrationally excited OH(X, $v \leq 13$) products. The other decay pathway opens for H_2O ($\tilde{C}$) molecules in levels with $\langle J_a \rangle^2 > 0$. This relies on the heterogeneous (Coriolis-induced) coupling to the $\tilde{B}$ state PES and results in both ground and electronically excited state OH fragments with very high rotational but minimal vibrational excitation. At shorter excitation wavelengths of around 122 nm, the electronic state ($\tilde{D}$) can be reached. Dissociation from the $\tilde{D}$ state efficiently undergoes a fast conversion to the $\tilde{B}$ state surface via an avoided crossing at a bent geometry.[51−53]

The next intense features of the absorption spectrum of H_2O correspond to the 3d Rydberg series, which have been studied experimentally with rotational resolution.[54,55] The optically allowed members of the 3d series appear as three electronic bands, as displayed in Figure 1. The spectrum around 113.0−112.6 nm is assigned to the $\tilde{E}^1B_1$ state, associated with the electron transition $3da_1 \leftarrow 1b_1$. The other two bands around 112.0−111.0 and 112.5−112.1 nm are assigned to the $\tilde{F}^1A_1$ ($3db_1 \leftarrow 1b_1$) or $\tilde{F}^1B_1$ ($3da_1' \leftarrow 1b_1$), and $\tilde{E}'^1B_2$ ($3da_2 \leftarrow 1b_1$) states, respectively. The photodissociation dynamics of these Rydberg states have been addressed recently. Wang et al.[56] reported the dissociation features of H_2O via the $\tilde{F}$ state at 111.5 nm using the VUV free electron laser (FEL), at the Dalian Coherent Light Source (DCLS). The observed OH(X) and OH(A) products with high rotational excitation were ascribed to a fast dissociation on the $\tilde{B}$ state surface after several internal conversions from the $\tilde{F}$ state to the $\tilde{B}$ state. Meanwhile, Yang et al.[57] measured the lifetimes of the $\tilde{F}^1A_1$ and $\tilde{F}^1B_1$ states of H_2O and proposed that the molecule on the $\tilde{F}^1A_1$ state mainly decays through the $\tilde{D}$ state followed by the fast conversion from the $\tilde{D}$ state to the $\tilde{B}$ state, while that on the $\tilde{F}^1B_1$ states decays through the $\tilde{F}^1A_1$ state via the Coriolis interaction. In contrast, the dissociation of H_2O via the $\tilde{E}$ state displayed exceptionally highly vibrationally excited OH(X) products, with a nascent vibrational state population distribution that peaks at v = 9 and extends to the highest vibrational level v = 15.[58]

Unlike the $\tilde{E}$ and $\tilde{F}$ states, however, the $\tilde{E}'$ state is very strong in absorption but very weak in fluorescence. Fillion et al.[54] suggested a fast predissociation mechanism via a linear $^1B_2$ ($3pb_2 \leftarrow 3a_1$) state from the initial excited $\tilde{E}'$ state, leading to "dark fragments". The dissociation dynamics of this state seem to be different and interesting, but the detailed features on the state-to-state level have not been available yet. Over the past 20 years, our group has revealed the photodissociation dynamics of H_2O on the initial excited $\tilde{A}$, $\tilde{B}$, $\tilde{C}$, $\tilde{D}$, $\tilde{E}$, and $\tilde{F}$ states systematically, by using the high-resolution H atom photofragment translational spectroscopy (PTS) method. In this work, we continue to investigate the dissociation dynamics of H_2O on the $\tilde{E}'$ state, using the PTS combined with the VUV FEL laser.[59−61] The results show exquisite features of H_2O photodissociation through 3d Rydberg states, and possible dissociation mechanisms have been discussed.

2. METHODS

The experiments were performed on a recently constructed end-station for molecular photochemistry around the VUV FEL beamline at DCLS. Briefly, the VUV FEL facility operated in the HGHG mode,[62] where the seeding laser was injected to interact with the electron beam in the modulator. The seeding pulse at 240−360 nm was generated by an ultrafast laser system. The electron beam produced by a photocathode RF gun was accelerated to the beam energy of ∼300 MeV with a bunch charge of 500 pC. The microbunched beam was then sent through the radiator, which was tuned to the 2nd/3rd/4th harmonic of the seeding wavelength. Optimization of the linear accelerator yielded a high-quality electron beam with an emittance of ∼1.5 mm mrad, energy spread of ∼1‰, and pulse duration of ∼1.5 ps. The VUV FEL was operated at 10 Hz, with the maximum pulse energy >500 μJ/pulse. The output wavelength in the range 50−150 nm can be easily tuned, and the typical spectral bandwidth of the VUV FEL pulse was ∼50 cm^{-1}.

The H atom PTS was acquired by the H atom Rydberg tagging time-of-flight (TOF) technique,[63,64] the fundamental idea of which is the two-step excitation of the H atom. The first step involves VUV photon excitation of the H atom from the n = 1 ground state to the n = 2 state by absorbing one 121.6 nm photon. The second step concerns absorbing a UV (∼365 nm) photon exciting the H atom from n = 2 to a Rydberg state ($n \sim$ 30−80). The 121.6 nm radiation was generated by four wave difference frequency mixing using two 212.556 nm photons and one 845 nm photon. The 212.556 nm laser light was produced by doubling the output of a tunable dye laser operating at ∼425 nm, pumped by the third harmonic output of a Nd:YAG laser, while the 845 nm laser light was the direct output of another dye laser pumped by half of the second harmonic output from the same Nd:YAG laser. The 365 nm laser light was generated by doubling the output of a tunable dye laser operating at ∼730 nm, pumped by another half of the second harmonic output of the Nd:YAG laser. The FEL output crossed perpendicular to the molecular beam axis and polarized in the horizontal direction. TOF spectra along axes parallel and perpendicular to this polarization axis were thus measured by rotating the MCP detector. The 121.6 nm detection laser pulse caused some H_2O photodissociation. The TOF spectrum of these probe laser-induced H atoms was obtained by turning the VUV FEL beam on and off, and subtracted accordingly.

The charged species generated in the interaction region were extracted away by a small electric field (∼75 V/cm) mounted perpendicular with the detection direction. The Rydberg H

https://doi.org/10.1021/acs.jpca.1c01459
J. Phys. Chem. A XXXX, XXX, XXX−XXX

atoms, after flying a certain distance, were then field ionized and detected by a Z-stack microchannel plate (MCP) detector mounted on a rotational detector. Then, the signal was amplified by a fast preamplifier and counted by a multichannel scaler.

3. RESULTS AND DISCUSSION

3.1. Product Translational Energy Distributions. We have recorded the H atom TOF spectra from H_2O photodissociation at 112.5 and 112.1 nm using the above experimental methods. The photolysis wavelengths chosen here have been marked in Figure 1. As reported by Fillion et al.,[54] the electronic absorption of the $\tilde{E}'$ state is very strong, but the fluorescence spectra ($OH(A \rightarrow X)$) are weak around 112.1 nm and are almost completely missing at around 112.5 nm. Our goal is to unravel the dynamical source of such differences between the absorption and fluorescence spectra at the $\tilde{E}'$ state. Figure 2 shows the TOF spectra at these two

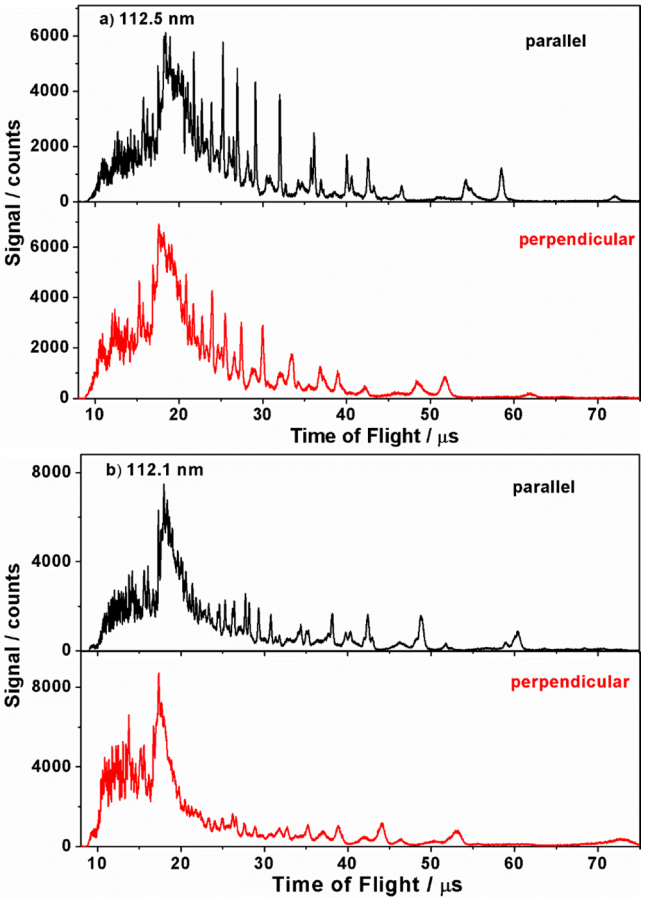

Figure 2. Time-of-flight spectra of H atom fragments from H_2O photolysis at (a) 112.5 nm and (b) 112.1 nm with the detection axis parallel (in black) and perpendicular (in red) to photolysis laser polarization.

wavelengths with the detection axis parallel (0°, in black) and perpendicular (90°, in red) to the photolysis laser polarization. It is noted that the H atom at the perpendicular direction contains the velocity of the molecular beam; thus, the arriving time is faster than that at the parallel direction. The TOF spectrum at the magic angle (~54.7°) was also recorded in order to make sure that the polarization direction is accurate. The TOF spectra have been converted to the PTS using the following equation:

$$E_T = \frac{1}{2} m_H \left(1 + \frac{m_H}{m_{OH}}\right)\left(\frac{d}{t}\right)^2 \quad (1)$$

where d is the flight distance of the H atom ($d \approx 280$ mm), and t is the measured time-of-flight. It is noted that the velocity of the parent molecule is also included in the conversion process. Figure 3 displays the product translational energy

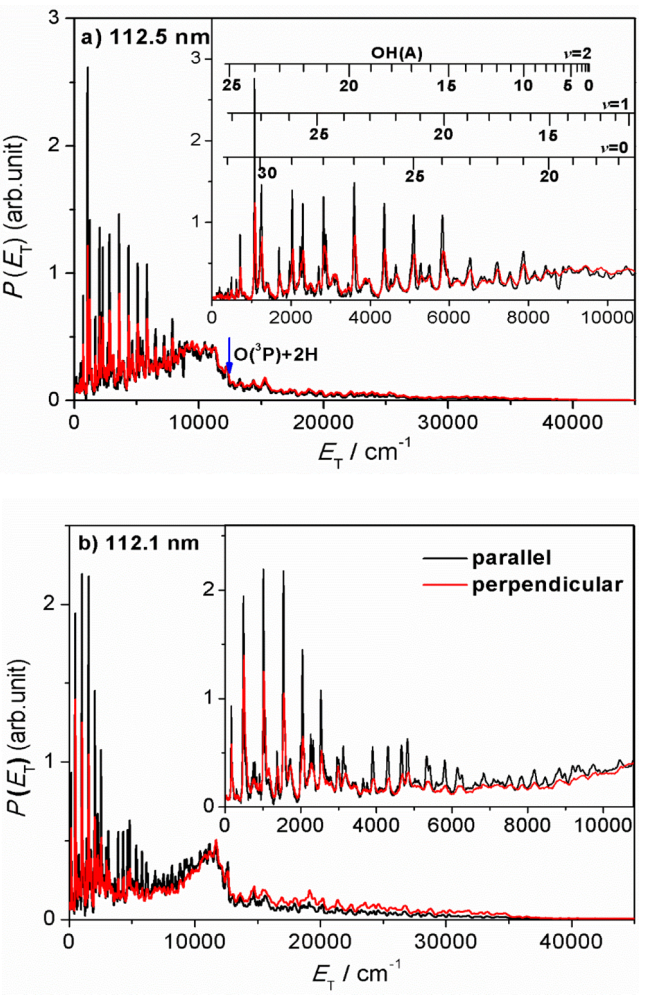

Figure 3. Translational energy spectra for the H atom fragments following photodissociation of H_2O at (a) 112.5 nm and (b) 112.1 nm, with the detection axis parallel (in black) or perpendicular (in red) to the photolysis laser polarization. The inset in panel a displays the assignment of the sharp structures. The maximum translational energy for the three-body dissociation channel $O(^3P)$ + 2H is also indicated in the panel.

distributions at the two wavelengths in the parallel and perpendicular directions, respectively. The dominant features observed in Figure 3 are extensive sharp structures in the low translational energy range, which correspond to the electronically excited OH(A) products. According to the total energy conservation in the photolysis process, most of these sharp features can be assigned to high rotational levels of OH(A, v = 0−2) products. For instance, the peaks around 1200 cm^{-1} from 112.5 nm photolysis have been ascribed to the populations of OH(A, v = 0, N = 30; v = 1, N = 27; and v

https://doi.org/10.1021/acs.jpca.1c01459
J. Phys. Chem. A XXXX, XXX, XXX−XXX

= 2, N = 24) rotational levels, respectively. The group of structures located at the higher translational energy range, corresponding to the ground electronic state OH(X) products, can still be observed, but with quite small populations. These structures are congested and partially resolved, which are different qualities from that observed in H_2O photodissociation on the lower-lying electronic states.[44] In addition to the OH(A) and OH(X) products, a broad underlying energy distribution has also been observed with the peak located at around 10 000 cm^{-1}, which can be ascribed as the three-body dissociation $O(^3P)$ + 2H channel. The translational energy distributions from 112.1 nm photolysis have similar profiles with those from 112.5 nm photolysis, suggesting similar dissociation dynamics.

From the translational energy distributions obtained above, the quantum state population distributions and the quantum state dependent anisotropy parameters can be determined. In the photodissociation process, the photofragment detected at any angle in the center-of-mass frame (θ_{cm}) relative to the photolysis light polarization can be represented using the following equation:

$$f(E_T, \theta_{cm}) = \sigma(E_T)\{1 + \beta(E_T)P_2(\cos\theta_{cm})\} \quad (2)$$

where $\sigma(E_T)$ is the product translational energy distribution, and $\beta(E_T)$ is the anisotropy parameter as a function of the translational energy, which depends on the details of the excitation and the decay of the molecule. In this experiment, the translational energy distributions at two directions were measured; therefore, $\beta(E_T)$ can be calculated.

3.2. OH Product Quantum State Distributions and Angular Distributions. According to the term values of all rovibrational quantum levels of OH(X) and OH(A) products, we have simulated the PTSs in the two polarizations. The Gaussian-like profiles were used to fit each OH rotational quantum state population, and the line widths of these profiles were assumed to be about 1% of the corresponding translational energy within a narrow range variation. Through tuning the peak intensity of each OH quantum state, the simulated PTS agreed well with the experimental one, as shown in Figure 4. The other simulated spectra are not shown here.

Figure 5 displays the rotational state distributions of the OH(A) products for v = 0−5. It is apparent that the rotational distribution fluctuates as a function of rotational quantum number. For OH(A, v = 0) products from 112.5 nm photolysis, they are highly rotationally excited, with strong populations at around N = 24−29. For OH(A, v = 1−3) products, the rotational state distributions are still strongly inverted, with peaks at N = 27, 24, and 21, close to the highest energetically accessible rotational levels, respectively, while the populations of OH(A, v = 4 and 5) fluctuate more strongly, with moderate rotational excitation. Figure 6a shows the vibrational distribution of the OH(A) products from 112.5 nm photolysis. The OH(A, v = 0−2) products are dominant, while the populations of OH(A) with vibrational excitation of v = 3−5 decrease almost linearly as the vibrational energy increases.

These quantum state populations of OH(A) products are quite surprising, since almost no OH(A) fluorescence at around 112.5 nm has been observed by Fillion and coworkers.[54] In this work, however, the OH(A) products should be dominant as displayed in Figure 3a. Such discrepancy may arise from the strong predissociation of highly rovibrationally excited OH(A) products. According to the theoretical

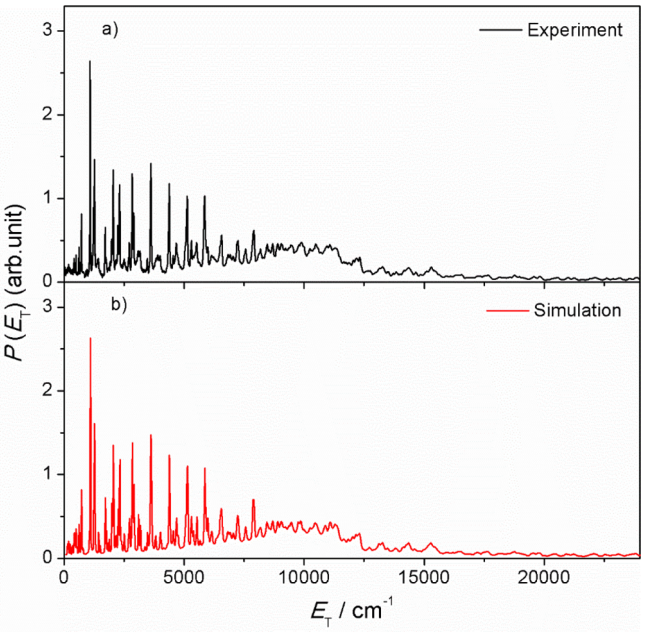

Figure 4. Experimental (a) and simulated (b) product translational energy distributions for H_2O photolysis at 112.5 nm with the detection axis parallel to photolysis laser polarization.

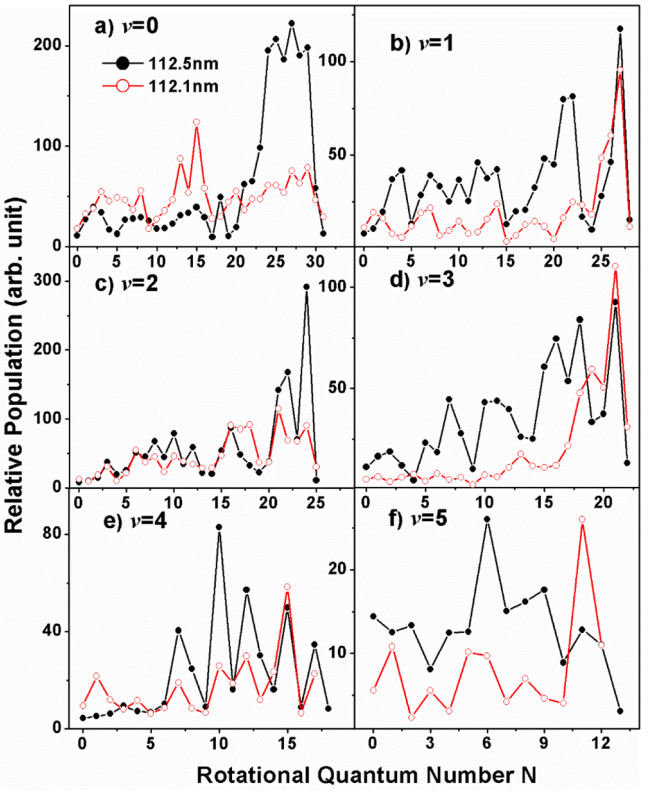

Figure 5. Rotational state distributions of the OH(A, v = 0−5) products from H_2O photolysis at 112.5 nm (in black) and 112.1 nm (in red).

calculations,[65,66] the $A^2\Sigma^+$ state of OH crosses with three repulsive states ($^4\Sigma^-$, $^2\Sigma^-$, and $^4\Pi$) in the Franck−Condon region and predissociates to $O(^3P)$ + H products via spin−orbit induced couplings with the three repulsive states. As determined by the locations of the crossings and the

https://doi.org/10.1021/acs.jpca.1c01459
J. Phys. Chem. A XXXX, XXX, XXX−XXX

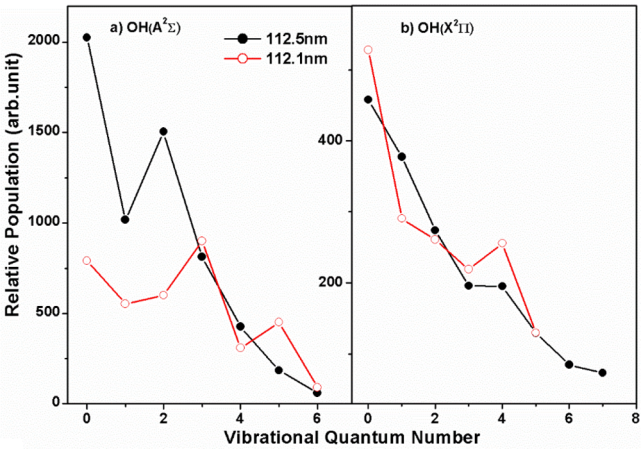

Figure 6. Vibrational state distributions of the OH(A) products (a) and OH(X) products (b) from H_2O photolysis at 112.5 nm (in black) and 112.1 nm (in red).

dissociation limit of $O(^3P)$ + H, high rotational states in $v = 0$, $N \geq 24$, and in $v = 1$, $N \geq 15$, of OH(A), and all rotational levels in $v = 2$ and $v = 3$ predissociate primarily via the $^4\Sigma^-$ state, while those in $v = 4$ and 5 decompose via the $^4\Sigma^-$, $^2\Sigma^-$, and $^4\Pi$ states.[67] The predissociation processes compete with the radiative channels and strongly reduce the lifetimes and fluorescence yields of the corresponding OH(A) products. The rotational state distributions of OH(A) from 112.5 nm photolysis imply that almost 90% OH(A) products will predissociate, leading to the missing fluorescence. In comparison, the rotational state distributions of the OH(A, $v = 0$) products from 112.1 nm photolysis are moderate, with the peak around $N = 15$. These lower rotational states of OH(A) products would emit the fluorescence, which accords with the weak fluorescence spectra around 112.1 nm reported by Fillion et al.[54] Figure 6a also displays the vibrational distribution of the OH(A) products at 112.1 nm. A little hot vibrational excitation has been observed, suggesting different Coriolis coupling induced by parent rotational excitation between 112.1 and 112.5 nm.

We have also obtained the quantum state distributions of OH(X) products. The small signal in the corresponding translational energy spectra implies that the H + OH(X) channel is minor, and the partially resolved structure prevents determining the exact rotational state distributions. Figure 6b shows the vibrational state distributions of OH(X) products at 112.1 and 112.5 nm. The populations decrease as the vibrational energy increases, but the OH(X, $v = 0$) product

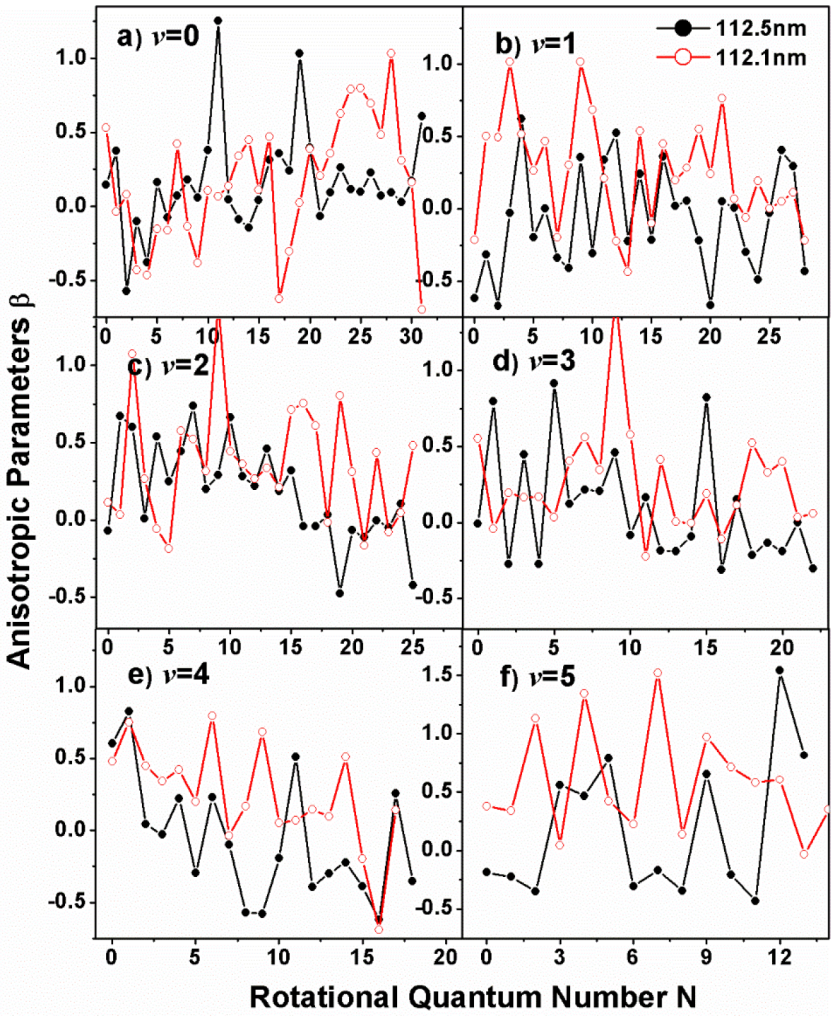

Figure 7. Rotational dependence of the anisotropy parameter β for the OH(A, $v = 0$–5) products from H_2O photolysis at 112.5 nm (in black) and 112.1 nm (in red).

https://doi.org/10.1021/acs.jpca.1c01459
J. Phys. Chem. A XXXX, XXX, XXX−XXX

Table 1. Branching Ratios for the Different Channels from H_2O Photolysis at Several Wavelengths

product channels	112.5 nm ($\tilde{E}'^1B_2$)	112.1 nm ($\tilde{E}'^1B_2$)	111.5 nm[56] ($\tilde{F}^1A_1/\tilde{F}^1B_1$)	112.8 nm[58] ($\tilde{E}^1B_1$)	121.6 nm[34] ($\tilde{B}^1A_1/\tilde{D}^1A_1$)
H + OH(A)	0.53	0.45	0.31	0.15	0.13
H + OH(X)	0.15	0.20	0.22	0.6	0.66
$O(^3P)$ + 2H	0.32	0.35	0.47	0.25	0.21

Scheme 1

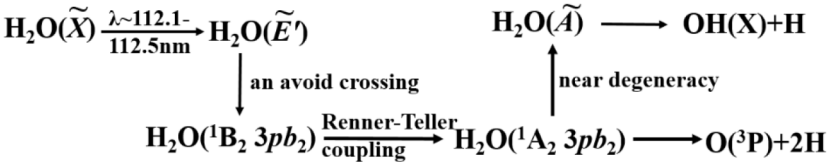

Scheme 2

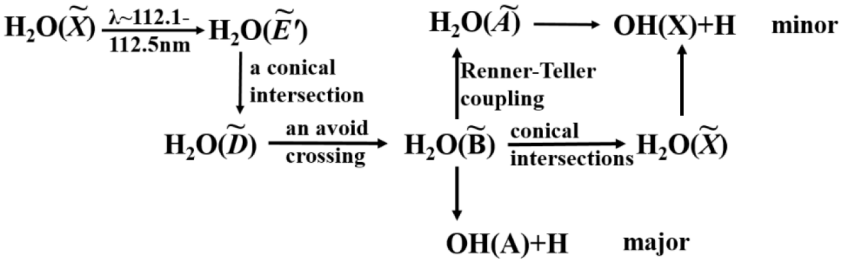

is no longer the most important single vibrational product channel, due to vibrationally excited OH products with $v = 1-7$ having a modest population. This is different from that observed in H_2O photodissociation at 121.6 nm; i.e., approximately half the total OH(X) population in $v = 0$ was observed.[34]

Figure 7 displays the rotational state specific anisotropy parameter $\beta(N)$ distributions of the OH(A, $v = 0-5$) products at 112.1 and 112.5 nm, respectively. The variations in β are quite different from each other. There are no general features for these distributions. The anisotropy parameter fluctuates around zero with some high positive or negative values. This probably arises because the generation of these products requires the experience of different angular forces during the dissociation.

Branching ratios for the different channels were also obtained based on the careful simulations to these experimental results and the assumption that the broad distribution above the energetic limit is all from the triple product channel. Integrating the areas under the respective distributions returns relative H atom yields for the three channels. Recognizing that two H atoms are formed in the $O(^3P)$ + 2H channel, the relative H atom yields are used to determine the branching ratio (Table 1).

The relative branching ratio to OH(A) and OH(X) was determined through the simulations to be about 3.5:1 at 112.5 nm and 2.25:1 at 112.1 nm. These are quite different from that observed in H_2O photodissociation at 121.6 nm, in which the ratio of 1:5 was obtained.[34] It is worth noting that the branching ratios for H_2O photolysis from different 3*d* Rydberg series are also quite different, suggesting the complex nature of H_2O potential surfaces.

3.3. Dissociation Mechanisms. We now seek to reveal the complicated photodissociation mechanisms. As we know, the Rydberg spectrum of H_2O is one of the best characterized of any polyatomic species and can be considered in many respects as a model. The most intense features around 114−111 nm, corresponding to the 3*d* complex, are the starting point of dipole-allowed $nd \leftarrow 1b_1$ Rydberg series. A previous high-resolution study of the water absorption reported that the striking difference between the absorption and fluorescence spectra appears at the $\tilde{E}'$ state, which is very strong in absorption but is almost completely missing in fluorescence.[54] In contrast, other 3*d* components ($\tilde{E}$ and $\tilde{F}$ states) display an intense fluorescence signal corresponding to the whole rotational band profile, suggesting complicated dissociation mechanisms of 3*d* series.

Theoretical calculations[68] pointed out that the equilibrium geometry of the $\tilde{E}'$ state is bent with the bond angle larger than that for the ground state of water. Gilbert et al.[69] proposed a bent−linear interaction between the $\tilde{E}'$ state and the $^1B_2$ $3pb_2$ state, the state of which has a quasilinear geometry and arises from the excitation of the $3a_1$ orbit. Thus, the water molecule can undergo a fast conversion from the initial excited $\tilde{E}'$ state to the $^1B_2$ state via an avoided crossing between them in the region of 120° and then predissociate to the dissociative $^1A_2 3pb_2$ state due to the Renner−Teller coupling between the $^1B_2$ and $^1A_2$ states. The molecules on the $^1A_2$ state can dissociate toward the $O(^3P)$ + 2H products or further couple to the $\tilde{A}$ state yielding rovibrationally excited OH(X) products,[48] both of which are "dark channels". The processes are illustrated as Scheme 1.

In addition, David et al.[68] reported that the $\tilde{E}'$ and $\tilde{D}$ states cross at about 140° with C_{2v} symmetry. There is a conical intersection between the $\tilde{E}'$ and $\tilde{D}$ states located at $R_{OH} = 0.96$ Å and $\theta_{HOH} = 139.8°$. Thus, the alternative predissociation route would be an internal conversion from the initial excited $\tilde{E}'$ state to the $\tilde{D}$ state. It is well-known that an avoided crossing between the $\tilde{B}$ and $\tilde{D}$ states located at the bond angle of about 100°, which is close to the Franck−Condon region with a bond angle of 104°, leads to a fast electronically nonadiabatic transition from the $\tilde{D}$ state to the $\tilde{B}$ state, and the

https://doi.org/10.1021/acs.jpca.1c01459
J. Phys. Chem. A XXXX, XXX, XXX−XXX

following dynamics are similar to those from the initial excited $\tilde{B}$ state.[51] Such processes are illustrated in Scheme 2. The dominant OH(A) products observed in this work suggest that Scheme 2 plays a major role in the photodissociation process from the $\tilde{E}'$ state. Though this channel is a "bright channel", the strong predissociation of highly rotationally excited OH(A) diminishes the fluorescence.

4. CONCLUSION

In this paper, the H atom translational energy distributions at 112.5 and 112.1 nm were measured using the H atom Rydberg tagging TOF technique combined with the VUV FEL laser. Analysis of the energy disposal shows that OH(X) and OH(A) fragments are all highly rotationally excited and moderately vibrationally excited. Two possible dissociation pathways are discussed. One is the fast transition from the initial excited $\tilde{E}'$ state to the $\tilde{D}$ state, followed by further transitions to the lower-lying states; the other is the conversion from the $\tilde{E}'$ state to the $^1A_2$ state, mediated by the $^1B_2$ $3pb_2$ state through a bent−linear interaction. The present study would deepen our understanding about dissociation from 3*d* Rydberg states of polyatomic molecules.

AUTHOR INFORMATION

Corresponding Authors

Xueming Yang − *State Key Laboratory of Molecular Reaction Dynamics and Dalian Coherent Light Source, Dalian Institute of Chemical Physics, Chinese Academy of Sciences, Dalian 116023, P. R. China; Department of Chemistry, College of Science, Southern University of Science and Technology, Shenzhen 518055, P. R. China;* orcid.org/0000-0001-6684-9187; Email: xmyang@dicp.ac.cn

Kaijun Yuan − *State Key Laboratory of Molecular Reaction Dynamics and Dalian Coherent Light Source, Dalian Institute of Chemical Physics, Chinese Academy of Sciences, Dalian 116023, P. R. China;* orcid.org/0000-0002-5108-8984; Email: kjyuan@dicp.ac.cn

Authors

Zijie Luo − *Department of Physics, School of Science, Dalian Maritime University, Dalian, Liaoning 116026, P. R. China; State Key Laboratory of Molecular Reaction Dynamics and Dalian Coherent Light Source, Dalian Institute of Chemical Physics, Chinese Academy of Sciences, Dalian 116023, P. R. China*

Yao Chang − *State Key Laboratory of Molecular Reaction Dynamics and Dalian Coherent Light Source, Dalian Institute of Chemical Physics, Chinese Academy of Sciences, Dalian 116023, P. R. China*

Yarui Zhao − *State Key Laboratory of Molecular Reaction Dynamics and Dalian Coherent Light Source, Dalian Institute of Chemical Physics, Chinese Academy of Sciences, Dalian 116023, P. R. China*

Jiayue Yang − *State Key Laboratory of Molecular Reaction Dynamics and Dalian Coherent Light Source, Dalian Institute of Chemical Physics, Chinese Academy of Sciences, Dalian 116023, P. R. China*

Zhichao Chen − *State Key Laboratory of Molecular Reaction Dynamics and Dalian Coherent Light Source, Dalian Institute of Chemical Physics, Chinese Academy of Sciences, Dalian 116023, P. R. China*

Yi Cheng − *Department of Physics, School of Science, Dalian Maritime University, Dalian, Liaoning 116026, P. R. China*

Li Che − *Department of Physics, School of Science, Dalian Maritime University, Dalian, Liaoning 116026, P. R. China*

Guorong Wu − *State Key Laboratory of Molecular Reaction Dynamics and Dalian Coherent Light Source, Dalian Institute of Chemical Physics, Chinese Academy of Sciences, Dalian 116023, P. R. China;* orcid.org/0000-0002-0212-183X

Complete contact information is available at: https://pubs.acs.org/10.1021/acs.jpca.1c01459

Author Contributions

‖Z. Luo and Y. Chang contributed equally.

Notes

The authors declare no competing financial interest.

ACKNOWLEDGMENTS

The experimental work is supported by the Chemical Dynamics Research Center (Grant 21688102), the National Natural Science Foundation of China (NSFC 21873099, 21922306, 21590802), the Key Technology Team of the Chinese Academy of Sciences (Grant GJJSTD20190002), the international partnership program of Chinese Academy of Sciences (121421KYSB20170012), and Liaoning Revitalization Talents Program (XLYC1907154). We also thank the staff team of the Dalian Coherent Light Source (DCLS) for technique support.

REFERENCES

(1) Hu, X. X.; Zhou, L. S.; Xie, D. Q. State-to-State Photodissociation Dynamics of the Water Molecule. *Wires Comput. Mol. Sci.* **2018**, *8*, No. e1350.

(2) van Dishoeck, E. F.; Herbst, E.; Neufeld, D. A. Interstellar Water Chemistry: From Laboratory to Observations. *Chem. Rev.* **2013**, *113*, 9043−9085.

(3) Yang, X. M. State-to-State Dynamics of Elementary Chemical Reactions Using Rydberg H-atom Translational Spectroscopy. *Int. Rev. Phys. Chem.* **2005**, *24*, 37−98.

(4) Lee, L. C.; Suto, M. Quantitative Photoabsorption and Fluorescence Study of H_2O and D_2O at 50−190 nm. *Chem. Phys.* **1986**, *110*, 161−169.

(5) Weide, K.; Kuhl, K.; Schinke, R. Unstable Periodic-Orbits, Recurrences, and Diffuse Vibrational-Structures in the Photodissociation of Water Near 128 nm. *J. Chem. Phys.* **1989**, *91*, 3999−4008.

(6) Wang, H. T.; Felps, W. S.; Mcglynn, S. P. Molecular Rydberg States. VII. Water. *J. Chem. Phys.* **1977**, *67*, 2614−2628.

(7) Engel, V.; Schinke, R.; Staemmler, V. Photodissociation Dynamics of H_2O and D_2O in the First Absorption Band: A Complete Ab Initio Treatment. *J. Chem. Phys.* **1988**, *88*, 129−148.

(8) Guo, H.; Murrell, J. N. Dynamics of the $\tilde{A}$-State Photodissociation of H_2O at 193 nm. *Mol. Phys.* **1988**, *65*, 821−827.

(9) Zhang, J. Z.; Imre, D. G. Spectroscopy and Photodissociation Dynamics of H_2O: Time-Dependent View. *J. Chem. Phys.* **1989**, *90*, 1666−1676.

(10) Engel, V.; Staemmler, V.; Vanderwal, R. L.; Crim, F. F.; Sension, R. J.; Hudson, B.; Andresen, P.; Hennig, S.; Weide, K.; Schinke, R. Photodissociation of Water in the First Absorption Band: A Prototype for Dissociation on A Repulsive Potential Energy Surface. *J. Phys. Chem.* **1992**, *96*, 3201−3213.

(11) Hwang, D. W.; Yang, X. F.; Yang, X. M. The Vibrational Distribution of the OH Product from H_2O Photodissociation at 157 nm: Discrepancies between Theory and Experiment. *J. Chem. Phys.* **1999**, *110*, 4119−4122.

(12) van Harrevelt, R.; van Hemert, M. C. Photodissociation of Water in the $\tilde{A}$ Band Revisited with New Potential Energy Surfaces. *J. Chem. Phys.* **2001**, *114*, 9453−9462.
(13) Lu, I. C.; Wang, F. Y.; Yuan, K. J.; Cheng, Y.; Yang, X. M. Nonstatistical Spin Dynamics in Photodissociation of H_2O at 157 nm. *J. Chem. Phys.* **2008**, *128*, 066101.
(14) Zhou, L. S.; Xie, D. Q.; Sun, Z. G.; Guo, H. Product Fine-Structure Resolved Photodissociation Dynamics: The A Band of H_2O. *J. Chem. Phys.* **2014**, *140*, 024310.
(15) Yang, X. F.; Hwang, D. W.; Lin, J. J.; Ying, X. Dissociation Dynamics of the Water Molecule on $\tilde{A}$ ($\sim$1)B_1 Electronic Surface. *J. Chem. Phys.* **2000**, *113*, 10597−10604.
(16) van Harrevelt, R.; van Hemert, M. C. Photodissociation of Water. I. Electronic Structure Calculations for the Excited States. *J. Chem. Phys.* **2000**, *112*, 5777−5786.
(17) van Harrevelt, R.; van Hemert, M. C. Photodissociation of Water. II. Wave Packet Calculations for the Photofragmentation of H_2O and D_2O in $\tilde{B}$ Band. *J. Chem. Phys.* **2000**, *112*, 5787−5808.
(18) Krautwald, H. J.; Schnieder, L.; Welge, K. H.; Ashfold, M. N. R. Hydrogen-Atom Photofragment Spectroscopy. Photodissociation Dynamics of H_2O in the B-X Absorption Band. *Faraday Discuss. Chem. Soc.* **1986**, *82*, 99−110.
(19) Weide, K.; Schinke, R. Photodissociation Dynamics of Water in the Second Absorption Band. I. Rotational State Distributions of OH($^2\Sigma$) and OH($^2\Pi$). *J. Chem. Phys.* **1987**, *87*, 4627−4633.
(20) Guo, H. The $\tilde{B}$ -state Photodissociation of Water. *Mol. Phys.* **1989**, *68*, 249−254.
(21) Weide, K.; Schinke, R. Photodissociation Dynamics of Water in the Second Absorption Band. II. Ab Initio Calculation of the Absorption Spectra for H_2O and D_2O and Dynamical Interpretation of "Diffuse Vibrational" Structures. *J. Chem. Phys.* **1989**, *90*, 7150−7163.
(22) Zhou, L. S.; Jiang, B.; Xie, D. Q.; Guo, H. State-to-State Photodissociation Dynamics of H_2O in the B Band: Competition between Two Coexisting Nonadiabatic Pathways. *J. Phys. Chem. A* **2013**, *117*, 6940−6947.
(23) Zhou, L. S.; Xie, D. Q.; Guo, H. Signatures of Non-Adiabatic Dynamics in the Fine-Structure State Distributions of the OH($\tilde{X}$ /$\tilde{A}$) Products in the B-Band Photodissociation of H_2O. *J. Chem. Phys.* **2015**, *142*, 124317.
(24) Cheng, Y.; Cheng, L. N.; Guo, Q.; Yuan, K. J.; Dai, D. X.; Yang, X. M. Photodissociation Dynamics of D_2O Via the $\tilde{B}$ ($^1A_1$) Electronic State. *J. Chem. Phys.* **2011**, *134*, 104305.
(25) Vondirke, M.; Heumann, B.; Kuhl, K.; Schroder, T.; Schinke, R. Fluctuations in Absorption Spectra and Final Product State Distributions Following Photodissociation Processes. *J. Chem. Phys.* **1994**, *101*, 2051−2068.
(26) Zanganeh, A. H.; Fillion, J. H.; Ruiz, J.; Castillejo, M.; Lemaire, J. L.; Shafizadeh, N.; Rostas, F. Photodissociation of H_2O and D_2O Below 132 nm. *J. Chem. Phys.* **2000**, *112*, 5660−5671.
(27) Fillion, J. H.; van Harrevelt, R.; Ruiz, J.; Castillejo, N.; Zanganeh, A. H.; Lemaire, J. L.; van Hemert, M. C.; Rostas, F. Photodissociation of H_2O and D_2O in $\tilde{B}$, $\tilde{C}$, and $\tilde{D}$ States (134−119 nm). Comparison between Experiment and Ab Initio Calculations. *J. Phys. Chem. A* **2001**, *105*, 11414−11424.
(28) Harich, S. A.; Yang, X. F.; Yang, X.; van Harrevelt, R.; van Hemert, M. C. Single Rotational Product Propensity in the Photodissociation of HOD. *Phys. Rev. Lett.* **2001**, *87*, 263001.
(29) Harich, S. A.; Yang, Y. F.; Yang, X. M. Extremely Rotationally Excited OH from Water (HOD) Photodissociation through Conical Intersection. *Phys. Rev. Lett.* **2001**, *87*, 253201.
(30) Cheng, Y.; Yuan, K. J.; Cheng, L. N.; Guo, Q.; Dai, D. X.; Yang, X. M. Photodissociation Dynamics of H_2O: Effect of Unstable Resonances on the $\tilde{B}$ $^1A_1$ Electronic State. *J. Chem. Phys.* **2011**, *134*, 064301.
(31) Zhou, L. S.; Lin, G. S. M.; Xie, D. Q. State to State Photodissociation Dynamics of D_2O in the B Band. *J. Chem. Phys.* **2013**, *139*, 114303.
(32) Su, S.; Wang, H. Z.; Chen, Z. C.; Yu, S. R.; Dai, D. X.; Yuan, K. J.; Yang, X. M. Photodissociation Dynamics of HOD Via the $\tilde{B}$ ($^1A_1$) Electronic State. *J. Chem. Phys.* **2015**, *143*, 184305.
(33) Harich, S. A.; Yang, X. F.; Hwang, D. W. H.; Lin, J. J.; Yang, X. M.; Dixon, R. N. Photodissociation of D_2O at 121.6 nm: A State-to-State Dynamical Picture. *J. Chem. Phys.* **2001**, *114*, 7830−7837.
(34) Harich, S. A.; Hwang, D. W. H.; Yang, X. F.; Lin, J. J.; Yang, X. M.; Dixon, R. N. Photodissociation of H_2O at 121.6 nm: A State-to-State Dynamical Picture. *J. Chem. Phys.* **2000**, *113*, 10073−10090.
(35) Mordaunt, D. H.; Ashfold, M. N. R.; Dixon, R. N. Dissociation Dynamics of $H_2O(D_2O)$ Following Photoexcitation at the Lyman-Alpha Wavelength (121.6 nm). *J. Chem. Phys.* **1994**, *100*, 7360−7375.
(36) Yi, W. K.; Park, J.; Lee, J. Photodissociation Dynamics of Water at Lyman Alpha (121.6 nm). *Chem. Phys. Lett.* **2007**, *439*, 46−49.
(37) Dixon, R. N.; Hwang, D. W.; Yang, X. F.; Harich, S.; Lin, J. J.; Yang, X. Chemical "Double Slits": Dynamical Interference of Photodissociation Pathways in Water. *Science* **1999**, *285*, 1249−1253.
(38) Jiang, B.; Xie, D.; Guo, H. State-to-State Photodissociation Dynamics of Triatomic Molecules: H_2O in the B Band. *J. Chem. Phys.* **2012**, *136*, 034302.
(39) Jiang, B.; Xie, D. Q.; Guo, H. Communication: State-to-State Differential Cross Sections for $H_2O(\tilde{B})$ Photodissociation. *J. Chem. Phys.* **2011**, *134*, 231103.
(40) Ashfold, M. N. R.; Bayley, J. M.; Dixon, R. N. Molecular Predissociation Dynamics Revealed through Multiphoton Ionization Spectroscopy. I. The $\tilde{C}^1B_1$ States of H_2O and D_2O. *Chem. Phys.* **1984**, *84*, 35−50.
(41) Hodgson, A.; Simons, J. P.; Ashfold, M. N. R.; Bayley, J. M.; Dixon, R. N. Quantum-State-Selected Photodissociation of H_2O-($\tilde{C}^1B_1$). *Chem. Phys. Lett.* **1984**, *107*, 1−5.
(42) Kuge, H. H.; Kleinermanns, K. Rotational Predissociation of $H_2O(\tilde{C}^1B_1)$ Studied by Multiphoton Ionization Spectroscopy in a Supersonic Free Jet. *J. Chem. Phys.* **1989**, *90*, 46−52.
(43) Yang, C. H.; Sarma, G.; ter Meulen, J. J.; Parker, D. H.; Western, C. M. REMPI Spectroscopy and Predissociation of the $\tilde{C}^1B_1$ (ν=0) Rotational Levels of H_2O, HOD and D_2O. *Phys. Chem. Chem. Phys.* **2010**, *12*, 13983−13991.
(44) Yuan, K. J.; Dixon, R. N.; Yang, X. M. Photochemistry of the Water Molecule: Adiabatic versus Nonadiabatic Dynamics. *Acc. Chem. Res.* **2011**, *44*, 369−378.
(45) Cheng, L. A.; Yuan, K. J.; Cheng, Y.; Guo, Q.; Yang, X. M.; Dixon, R. N. Product Rotational Franck-Condon Oscillations in HOD (J_{ka}, K_c) Dissociation. *Mol. Phys.* **2010**, *108*, 905−914.
(46) Yuan, K. J.; Cheng, Y.; Cheng, L.; Guo, Q.; Dai, D. X.; Wang, X. Y.; Yang, X. M.; Dixon, R. N. Nonadiabatic Dissociation Dynamics in H_2O: Competition between Rotationally and Nonrotationally Mediated Pathways. *Proc. Natl. Acad. Sci. U. S. A.* **2008**, *105*, 19148−19153.
(47) Yuan, K. J.; Cheng, L. N.; Cheng, Y.; Guo, Q.; Dai, D. X.; Yang, X. M. Tunable VUV Photochemistry Using Rydberg H-Atom Time-of-Flight Spectroscopy. *Rev. Sci. Instrum.* **2008**, *79*, 124101.
(48) Dixon, R. N.; Oliver, T. A. A.; Cheng, L.; Cheng, Y.; Yuan, K. J.; Yang, X. M. Vibronically Induced Decay Paths from the $\tilde{C}^1B_1$ -State of Water and Its Isotopomers. *J. Chem. Phys.* **2013**, *138*, 104306.
(49) Cheng, Y.; Cheng, L. N.; Guo, Q.; Yuan, K. J.; Dai, D. X.; Wang, X. Y.; Dixon, R. N.; Yang, X. M. Rotational State Specific Dissociation Dynamics of D_2O via the $\tilde{C}$ Electronic State. *J. Chem. Phys.* **2010**, *133*, 034307.
(50) Chang, Y.; Chen, Z. C.; Zhou, J. M.; Luo, Z. J.; He, Z. G.; Wu, G. R.; Ashfold, M. N. R.; Yuan, K. J.; Yang, X. M. Striking Isotopologue-Dependent Photodissociation Dynamics of Water Molecules: The Signature of an Accidental Resonance. *J. Phys. Chem. Lett.* **2019**, *10*, 4209−4214.
(51) Chang, Y.; Zhou, J. M.; Luo, Z. J.; Chen, Z. C.; He, Z. G.; Yu, S. R.; Che, L.; Wu, G. R.; Wang, X. A.; Yuan, K. J.; et al. Photodissociation Dynamics of H_2O and D_2O via the $\tilde{D}$ $^1A_1$ Electronic State. *Phys. Chem. Chem. Phys.* **2020**, *22*, 4379−4386.

https://doi.org/10.1021/acs.jpca.1c01459
J. Phys. Chem. A XXXX, XXX, XXX−XXX

(52) Yuan, K. J.; Cheng, L. N.; Cheng, Y.; Guo, Q.; Dai, D. X.; Yang, X. M. Two-Photon Photodissociation Dynamics of H_2O via the $\tilde{D}$ Electronic State. *J. Chem. Phys.* **2009**, *131*, 074301.
(53) He, Z. G.; Yang, D. Y.; Chen, Z. C.; Yuan, K. J.; Dai, D. X.; Wu, G. R.; Yang, X. M. An Accidental Resonance Mediated Predissociation Pathway of Water Molecules Excited to the Electronic $\tilde{C}$ State. *Phys. Chem. Chem. Phys.* **2017**, *19*, 29795−29800.
(54) Fillion, J. H.; Ruiz, J.; Yang, X. F.; Castillejo, M.; Rostas, F.; Lemaire, J. L. High Resolution Photoabsorption and Photofragment Fluorescence Spectroscopy of Water between 10.9 and 12 eV. *J. Chem. Phys.* **2004**, *120*, 6531−6541.
(55) Ashfold, M. N. R.; Bayley, J. M. Characterisation of the $\tilde{E}\ ^1B_1$ Rydberg State of Water by Resonance-Enhanced Multiphoton Ionisation (MPI) Spectroscopy. *J. Chem. Soc., Faraday Trans.* **1990**, *86*, 213−214.
(56) Wang, H. L.; Yu, Y.; Chang, Y.; Su, S.; Yu, S. R.; Li, Q. M.; Yang, J. Y.; Wang, X. A.; Zhang, W. Q.; Dai, D. X.; et al. Photodissociation Dynamics of H_2O at 111.5 nm by a Vacuum Ultraviolet Free Electron Laser. *J. Chem. Phys.* **2018**, *148*, 124301.
(57) Yang, D. Y.; Min, Y. J.; Chen, Z.; He, Z. G.; Chen, Z. C.; Yuan, K. J.; Dai, D. X.; Wu, G. R.; Yang, X. M. Ultrafast Dynamics of Water Molecules Excited to Electronic $\tilde{F}$ States: A Time-Resolved Photoelectron Spectroscopy Study. *Chin. J. Chem. Phys.* **2019**, *32*, 53−58.
(58) Chang, Y.; Li, Q. M.; An, F.; Luo, Z. J.; Zhao, Y. R.; Hu, X. X.; Xie, D. Q.; Plane, J. M. C.; Feng, W. H.; Western, C. M.; et al. Water Photolysis and Its Contributions to the Hydroxyl Dayglow Emissions in the Atmospheres of Earth and Mars. *J. Phys. Chem. Lett.* **2020**, *11*, 9086−9092.
(59) Zhou, J. M.; Zhao, Y. R.; Hansen, C. S.; Yang, J. Y.; Chang, Y.; Dai, D. X.; Western, C. M.; Ashfold, M. N. R.; Yuan, K. J.; Yang, X. M. Ultraviolet Photolysis of H_2S and Its Implications for SH Radical Production in the Interstellar Medium. *Nat. Commun.* **2020**, *11*, 1547.
(60) Chang, Y.; Yu, S. R.; Li, Q. M.; Yu, Y.; Wang, H. L.; Su, S.; Chen, Z. C.; Che, L.; Wang, X. A.; Zhang, W. Q.; et al. Tunable VUV Photochemistry Using Vacuum Ultraviolet Free Electron Laser Combined with H-Atom Rydberg Tagging Time-of-Flight Spectroscopy. *Rev. Sci. Instrum.* **2018**, *89*, 063113.
(61) Chang, Y.; An, F.; Li, Q. M.; Luo, Z. J.; Che, L.; Yang, J. Y.; Chen, Z. C.; Zhang, W. Q.; Wu, G. R.; Hu, X. X.; et al. Electronically excited OH super-rotors from water photodissociation by using vacuum ultraviolet free-electron laser pulses. *J. Phys. Chem. Lett.* **2020**, *11*, 7617−7623.
(62) Yu, L. H.; Babzien, M.; Ben-Zvi, I.; DiMauro, L. F.; Doyuran, A.; Graves, W.; Johnson, E.; Krinsky, S.; Malone, R.; Pogorelsky, I.; et al. High-Gain Harmonic-Generation Free-Electron Laser. *Science* **2000**, *289*, 932−934.
(63) Chang, Y.; Yu, Y.; Wang, H. L.; Hu, X. X.; Li, Q. M.; Yang, J. Y.; Su, S.; He, Z. G.; Chen, Z. C.; Che, L.; et al. Hydroxyl Super Rotors from Vacuum Ultraviolet Photodissociation of Water. *Nat. Commun.* **2019**, *10*, 1250.
(64) Ashfold, M. N. R.; Yuan, K. J.; Yang, X. M. Perspective: The Development and Applications of H Rydberg Atom Translational Spectroscopy Methods. *J. Chem. Phys.* **2018**, *149*, 080901.
(65) Yarkony, D. R. A Theoretical Treatment of the Predissociation of the Individual Rovibronic Levels of $OH/OD(A^2\Sigma^+)$. *J. Chem. Phys.* **1992**, *97*, 1838−1849.
(66) Parlant, G.; Yarkony, D. R. A Theoretical Analysis of the State-Specific Decomposition of $OH(A^2\Sigma^+, v', N', F_1/F_2)$ Levels, Including the Effects of Spin-Orbit and Coriolis Interactions. *J. Chem. Phys.* **1999**, *110*, 363−376.
(67) Kalyanaraman, C.; Sathyamurthy, N. Photodissociation and Predissociation Processes in OH: A Time-Dependent Quantum Mechanical Study. *Chem. Phys.* **1994**, *187*, 219−225.
(68) Hirst, D. M.; Child, M. S. Ab Initio Bending Potential-Energy Curves for Rydberg States of H_2O. *Mol. Phys.* **1992**, *77*, 463−476.
(69) Gilbert, R. D.; Child, M. S.; Johns, J. W. C. Rotational Analysis and Assignment of the 3d ← $1b_1$ Rydberg Complex in H_2O and D_2O. *Mol. Phys.* **1991**, *74*, 473−495.

https://doi.org/10.1021/acs.jpca.1c01459
J. Phys. Chem. A XXXX, XXX, XXX−XXX